THE BELL SYSTEM TECHNICAL JOURNAL
Vol. 53, No. 8, October 1974
Printed in U.S.A.

Theory of the Single-Material Fiber

By D. MARCUSE

(Manuscript received March 6, 1974)

The term "single-material fiber" describes a dielectric optical waveguide made of only one type of glass. The theory of this waveguide is simplified by placing the structure between two perfectly conducting planes that have very little influence on the properties of the low-order modes.

The field distribution and propagation constant of the lowest-order mode are investigated and compared to an approximate theory.

I. INTRODUCTION

A dielectric optical waveguide made entirely of one type of material is called a "single-material fiber."[1] Figure 1 shows such a structure schematically. It may be regarded as a rectangular dielectric waveguide supported by two infinitely extended slabs made of the same material. Such a structure has been shown to be capable of supporting modes that are concentrated near the enlarged section of the waveguide and that do not lose power by energy seepage into the slabs.[1,2] Single-material fibers are usually made of pure fused silica. Since no other material is needed to form a waveguide, the low-loss properties of pure fused silica can be fully utilized.[3]

The single-material fiber has been described by means of an approximate theory by Marcatili.[1] The theory presented here serves the purposes of proving that truly guided modes do indeed exist in single-material fibers and of providing more precise solutions for comparison with the approximate theory.

An analysis of the guided modes of the single-material fiber is presented in this paper. The mode field is expressed as a superposition of the guided modes as well as the radiation modes of the two types of slabs. The enlarged region, henceforth called the core, can be regarded as a slab joined by narrower support slabs on either side. Since the radiation modes of the slabs have a continuous spectrum of eigenvalues[4,5] (propagation constants), their contribution to the total field

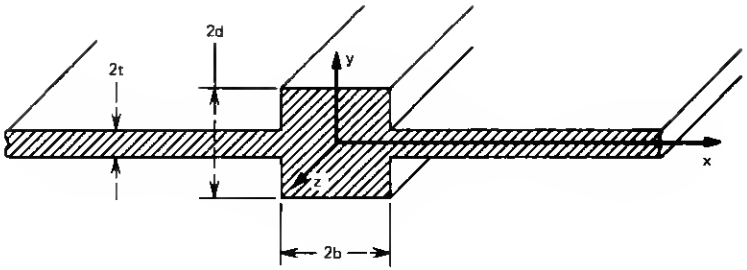

Fig. 1—Single-material fiber showing the rectangular core attached to its support slab.

consists of an integral that must be approximated by a sum for purposes of numerical analysis. In addition, the mathematical expression describing the guided and radiation modes are different so that the analysis becomes rather complex.

To simplify the analysis, it is convenient to consider the single-material fiber enclosed between two perfectly conducting planes, as shown in Fig. 2. Since the fields of the guided modes of the slabs, and hence the field of the guided mode of the fiber, are very tightly confined near the dielectric structure, the presence of the perfectly conducting planes does not appreciably influence the shape of horizontally polarized fields. However, the simplification of the analysis is considerable, since the modes that correspond to the guided modes of the open slab and the waveguide modes of the parallel plate system (corresponding to the radiation modes of the open slab) are now described by one analytical expression and belong to a system of discrete eigenvalues. There is, therefore, no need to worry about a suitable approximation to the integral over the radiation modes of the slabs. Vertically polarized fields (polarized in the y-direction) are strongly

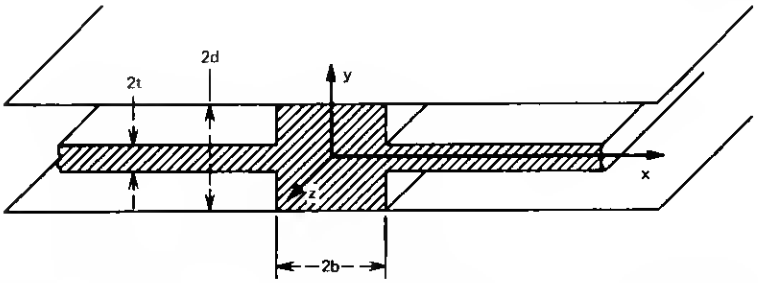

Fig. 2—For our analysis, the single-material fiber is placed between two perfectly conducting planes.

influenced by the presence of the metal plates, since the normal field components reach the metal plates with maximum intensity. For this reason, we limit the study of the single-material fiber to horizontally polarized modes. Vertically polarized modes could be treated if the perfectly conducting planes were replaced by magnetic short circuits. (An explanation of the negligible influence of the perfect conductors is given in the appendix.)

After formulating the exact solution to our problem, we present numerical approximations for the field distributions and the solution of the eigenvalue equation. The theory is compared to an approximate analysis.

II. CALCULATION OF THE MODES OF THE SINGLE-MATERIAL FIBER

The electric and magnetic fields of the modes of the single-material fiber are expressed as

$$\mathbf{E}^{(i)} = \sum_{\nu=1}^{\infty} c_\nu^{(i)} \mathcal{E}_\nu^{(i)} \tag{1}$$

and

$$\mathbf{H}^{(i)} = \sum_{\nu=1}^{\infty} c_\nu^{(i)} \mathcal{H}_\nu^{(i)}. \tag{2}$$

The script symbols indicate modes of the slabs. The superscript i assumes the values 1 and 2. Value 1 indicates modes of the wider slab that forms the core of the single-material fiber, while value 2 indicates the modes of the narrower supporting slabs.

The modes in the core region are those of a metallic parallel plate waveguide. These modes can be designated as TE modes with $\mathcal{E}_z^{(1)} = 0$ and TM modes with $\mathcal{H}_z^{(1)} = 0$. We have for the TE modes in region 1

$$\mathcal{E}_{z\nu}^{(1)} = 0 \tag{3}$$

and

$$\mathcal{H}_{z\nu}^{(1)} = \frac{A_\nu}{\omega\mu_0} \cos(k_{x\nu}x) \sin(k_{y\nu}y) e^{-i\beta z}. \tag{4}$$

We use odd integers, $\nu = 1, 3, \cdots$, to label these modes. In addition to the sine and cosine functions appearing in (4) we could also use the other three possible combinations. We restrict ourselves to the modes shown here, thus limiting ourselves to the study of fiber modes of a certain symmetry. All other modes can be obtained similarly.

The other field components can be obtained from $\mathcal{E}_z^{(1)}$ and $\mathcal{H}_z^{(1)}$ by differentiation (see, for example, page 13 of Ref. 4 or page 51 of Ref. 5).

The parameters appearing in (4) are related as

$$n^2k^2 = k_{x\nu}^2 + k_{y\nu}^2 + \beta^2, \tag{5}$$

with

$$k = \omega\sqrt{\epsilon_0\mu_0} = \frac{2\pi}{\lambda}. \tag{6}$$

The refractive index of the single-material fiber is designated by n and the refractive index of the medium outside the fiber is taken to be unity. The angular frequency is ω, and ϵ_0 and μ_0 are the dielectric permittivity and the magnetic permeability of vacuum.

The TM modes are labeled by even integers, $\nu = 2, 4, \cdots$, and are obtained from the field components

$$\mathcal{E}_{z\nu}^{(1)} = \frac{B_\nu}{\omega\epsilon_0} \sin(k_{x\nu}x) \cos(k_{y\nu}y)e^{-i\beta z} \tag{7}$$

and

$$\mathfrak{IC}_{z\nu}^{(1)} = 0. \tag{8}$$

TE and TM modes must satisfy the boundary conditions that $\mathcal{E}_{z\nu}^{(1)}$ and $\mathcal{E}_{x\nu}^{(1)}$ vanish at $y = \pm d$. These conditions are met if we use

$$k_{y\nu} = (2\mu_\nu - 1)\frac{\pi}{2d}. \tag{9}$$

Equations (5) and (9) are the same for TE modes (odd values of ν) and TM modes (even values of ν). The integers μ_ν assume the values

$$\begin{array}{lll} \mu_\nu = 1 & \text{for} & \nu = 1, 2 \\ \mu_\nu = 2 & \text{for} & \nu = 3, 4 \\ \mu_\nu = 3 & \text{for} & \nu = 5, 6 \\ \text{etc.} & & \end{array} \tag{10}$$

The TE and TM modes are mutually orthogonal. Their amplitude coefficients can be related to the amount of power in the core region by means of the equation

$$P = \frac{1}{2}\int_{-b}^{b} dx \int_{-d}^{d} dy(\mathcal{E}_\nu \times \mathfrak{IC}_\nu^*)_z. \tag{11}$$

The asterisk indicates complex conjugation, and the subscript z labels the z component of the vector. From (3), (4), and (11) we obtain

$$A_\nu = \left\{\frac{2\omega\mu_0(k_{y\nu}^2 + k_{x\nu}^2)^2 P}{\beta d\left|(k_{y\nu}^2 + k_{x\nu}^2)b + (k_{y\nu}^2 - k_{x\nu}^2)\dfrac{\sin 2k_{x\nu}b}{2k_{x\nu}}\right|}\right\}^{\frac{1}{2}}. \tag{12}$$

From (7), (8), and (11) follows also

$$B_\nu = \left\{ \frac{2\omega\epsilon_0(k_{y\nu}^2 + k_{x\nu}^2)^2 P}{n^2\beta d\left|(k_{y\nu}^2 + k_{x\nu}^2)b - (k_{y\nu}^2 - k_{x\nu}^2)\dfrac{\sin 2k_{x\nu}b}{2k_{x\nu}}\right|} \right\}^{\frac{1}{2}}. \tag{13}$$

It is apparent from (5) and (9) that $k_{x\nu}^2$ can assume positive as well as negative values.

We choose P equal to the unit of power. With this normalization, $|c_\nu^{(0)}|^2$ appearing in (1) and (2) measure directly the power carried by each mode.

Next, we turn to the modes of the narrower support slabs. Since the perfectly conducting planes do not touch the support slabs, their modes are more complicated. Strictly speaking, we do not have TE or TM modes with reference to the z direction. However, if we refer the labels TE or TM to the direction of propagation of the modes in the x–z plane, we do indeed have transverse electric and transverse magnetic modes. Used in this sense, we obtain the following z components of the TE modes of the support slabs:

$$\mathcal{E}_{z\nu}^{(2)} = \begin{cases} C_\nu e^{-i\sigma_{x\nu}(|x|-b)} \cos(\sigma_{y\nu}y) e^{-i\beta z} & |y| \leqq t \\ -C_\nu \dfrac{\cos \sigma_{y\nu}t}{\sin[\rho_\nu(d-t)]} e^{-i\sigma_{x\nu}(|x|-b)} \\ \qquad \times \sin[\rho_\nu(|y|-d)] e^{-i\beta z} & t \leqq |y| \leqq d \end{cases} \tag{14}$$

and

$$\mathcal{H}_{z\nu}^{(2)} = \begin{cases} \dfrac{\sigma_{y\nu}\beta}{i\sigma_{x\nu}\omega\mu_0} C_\nu e^{-i\sigma_{x\nu}(|x|-b)} \sin(\sigma_{y\nu}y) e^{-i\beta z} & |y| \leqq t \\ \dfrac{\sigma_{y\nu}\beta}{i\sigma_{x\nu}\omega\mu_0} C_\nu \dfrac{y}{|y|} \dfrac{\sin \sigma_{y\nu}t}{\cos \rho_\nu(d-t)} e^{-i\sigma_{x\nu}(|x|-b)} \\ \qquad \times \cos[\rho_\nu(|y|-d)] e^{-i\beta z} & t \leqq |y| \leqq d. \end{cases} \tag{15}$$

For TE modes, we have $\mathcal{E}_{y\nu}^{(2)} = 0$.

Maxwell's equations are satisfied if the parameters appearing in these field expressions satisfy the following relations:

$$n^2k^2 = \sigma_{x\nu}^2 + \sigma_{y\nu}^2 + \beta^2 \tag{16}$$

and

$$k^2 = \sigma_{x\nu}^2 + \rho_\nu^2 + \beta^2. \tag{17}$$

We again use odd integers ν to label the TE modes.

The field expressions satisfy the condition of vanishing tangential electric fields at the perfectly conducting planes. To satisfy the boundary conditions at the surface of the slab, the x dependence of the field expressions must be identical inside as well as outside the slab. For

this reason, the parameter $\sigma_{x\nu}$ is common to the fields for $t \geqq |y|$ and $t \leqq |y| \leqq d$. Since the fields must also satisfy boundary conditions along the planes $x = \pm b$ for all values of z, the parameter β must he the same for all field expressions, where β is the propagation constant for the mode of the single-material fiher that is yet to he determined.

The requirement of continuity of the field components $\mathcal{E}_{z\nu}^{(2)}$, $\mathcal{E}_{x\nu}^{(2)}$, $\mathcal{H}_{z\nu}^{(2)}$ and $\mathcal{H}_{x\nu}^{(2)}$ at $y = \pm t$ leads to the eigenvalue equation

$$\tan \sigma_{y\nu} t = \frac{\rho_\nu}{\sigma_{y\nu}} \cot [\rho_\nu (d - t)]. \tag{18}$$

Equation (18) determines the allowed values of $\sigma_{y\nu}$ and ρ_ν, since according to (16) and (17) we have

$$\rho_\nu^2 = \sigma_{y\nu}^2 - (n^2 - 1)k^2. \tag{19}$$

Although $\sigma_{y\nu}^2$ is always positive, ρ_ν^2 can he positive as well as negative. Modes with negative values of ρ_ν^2 correspond to the guided modes of an open slah. For negative values of ρ_ν^2, the cotangent function on the right-hand side of (18) hecomes a hyperbolic cotangent function that approaches unity for large values of its argument. The eigenvalue equation (18) is thus identical [for large values of $|\rho_\nu| (d - t)$] to the eigenvalue equation (8.3–16) on page 308 of Ref. 4 for even TE modes of the slah waveguide.

Modes with positive values of ρ_ν^2 correspond to the radiation modes of the open slah. However, instead of the continuous spectrum of radiation modes,[4,5] we now have a discrete spectrum of modes that approach the modes of the metallic parallel plate waveguide in the limit of vanishing slah thickness $2t$. The guided as well as the radiation modes of the narrow support slahs are thus represented hy the same analytical expressions (14) and (15). The presence of the perfectly conducting planes has the added advantage of causing the mode spectrum to he discrete.

The parameter $\sigma_{z\nu}^2$ can also he positive as well as negative. Positive values of $\sigma_{z\nu}^2$ correspond to real values of $\sigma_{z\nu}$, so that the mode fields (14) and (15) represent traveling waves that carry power away from the core region into the slah. Coupling the modes in the core region and the slah regions thus results in a leaky wave. It is clear that we ohtain guided single-material fiher modes only for negative values of $\sigma_{z\nu}^2$. We see from (16) that all $\sigma_{z\nu}^2$ are negative if σ_{z1}^2 of the lowest-order mode is negative, hecause the values of $\sigma_{y\nu}$ increase with increasing mode number. It is thus immediately apparent that lossless guided modes of the single-material fiher are indeed possible. Neither the guided modes

of the slab (those tightly confined to the slab region) nor the "unguided" modes, which correspond to the radiation modes of the open slab, carry away power; all decay exponentially in x direction. This argument is not changed when we let the metallic plates move to infinity so that we obtain a truly free single-material fiber. The single-material fiber is thus seen able to support guided modes whose fields are confined to the vicinity of the fiber core. The existence of these guided modes is contingent on sufficiently large values of β. Whether such solution with large β values really exist depends on the solutions that we must yet derive of the eigenvalue equation for β. However, even at this stage we can state that guided modes that do not suffer radiation losses are possible at least in principle.

Using (11), (14), and (15) we can again relate the amplitude coefficient to the power unit P:

$$C_\nu = \left\{ \frac{4\omega\mu_0 |\sigma_{x\nu}|^3 P}{\beta(\beta^2 + \sigma_{x\nu}^2) |t + \{\cos^2 \sigma_{y\nu} t / \sin^2 [\rho_\nu (d-t)]\}(d-t) - (n^2-1)k^2 \sin(2\sigma_{y\nu}t)/2\sigma_{y\nu}\rho_\nu^2|} \right\}^{\frac{1}{2}}. \quad (20)$$

The TM modes of the support slabs are labeled by even integers ν and follow from their z components:

$$\mathcal{E}_{z\nu}^{(2)} = \begin{cases} D_\nu e^{-i\sigma_{x\nu}(|x|-b)} \cos(\sigma_{y\nu} y) e^{-i\beta z} & |y| \leqq t \\ -D_\nu \dfrac{\cos \sigma_{y\nu} t}{\sin [\rho_\nu (d-t)]} e^{-i\sigma_{x\nu}(|x|-b)} \\ \qquad \times \sin [\rho_\nu (|y| - d)] e^{-i\beta z} & t \leqq |y| \leqq d, \end{cases} \quad (21)$$

$$\mathcal{H}_{z\nu}^{(2)} = \begin{cases} \dfrac{i\sigma_{x\nu} n^2 k^2}{\omega\mu_0 \beta \sigma_{y\nu}} D_\nu e^{-i\sigma_{x\nu}(|x|-b)} \sin(\sigma_{y\nu} y) e^{-i\beta z} & |y| \leqq t \\ \dfrac{i\sigma_{x\nu} n^2 k^2}{\omega\mu_0 \beta \sigma_{y\nu}} D_\nu \dfrac{\sin \sigma_{y\nu} t}{\cos [\rho_\nu (d-t)]} \dfrac{y}{|y|} e^{-i\sigma_{x\nu}(|x|-b)} \\ \qquad \times \cos [\rho_\nu (|y| - d)] e^{-i\beta z} & t \leqq |y| \leqq d. \end{cases} \quad (22)$$

For TM modes we have $\mathcal{H}_{y\nu}^{(2)} = 0$.

The parameters $\sigma_{x\nu}$, $\sigma_{y\nu}$, and ρ_ν are again related by (16), (17), and (19). The eigenvalue equation for TM modes is

$$\tan \sigma_{y\nu} t = \frac{1}{n^2} \frac{\sigma_{y\nu}}{\rho_\nu} \cot [\rho_\nu (d-t)]. \quad (23)$$

For large imaginary values of $\rho_\nu(d-t)$, (23) becomes the eigenvalue equation (8.3-45), page 313 of Ref. 4, for odd TM modes of the free slab.

Finally, we have

$$D_\nu = \left\{ \frac{4\omega\mu_0\beta\sigma_{y\nu}^2 |\sigma_{x\nu}|}{n^2k^2(\beta^2 + \sigma_{z\nu}^2)\left| t + n^2 \frac{\sin^2 \sigma_{y\nu} t}{\cos^2 [\rho_\nu (d-t)]} (d-t) + \frac{(n^2-1)k^2 \sin 2\sigma_{y\nu} t}{2\sigma_{y\nu}\rho_\nu^2} \right|} \right\}^{\frac{1}{2}}. \quad (24)$$

Now we have written down the field expressions for the mode fields that must he suhstituted into the series expansions (1) and (2) for the mode of the single-material fiher. It remains to match the field in the core of the single-material fiher to the field in the regions of the support slab. We need to require continuity of E_z, E_y, H_z, and H_y only along the line $x = b$ and $0 < y < d$, since the houndary conditions in the remaining three quadrants are satisfied for reasons of symmetry. Since the numerical analysis can handle only a finite numher of equations, we require continuity of the tangential field components only at a finite numher of points. Adjusting the size of the series expansion to the numher of matching points, we ohtain a finite, homogeneous equation system for the determination of the expansion coefficients $c_\nu^{(i)}$. This equation system can only have a solution if the determinant vanishes. The condition of vanishing system determinant provides the eigenvalue equation for the propagation constant β of the single-material fiber.

III. SPECIAL CASES AND APPROXIMATE SOLUTIONS

In the limit $t = 0$, an exact solution of the guided-mode prohlem is easily obtained. Since, in this case, the distrihutions of the fields in the two regions have the same y dependence, the houndary conditions along the plane $x = \pm b$ can he satisfied without resorting to the series expansions (1) and (2). Using the field expressions (3), (4), (7), (8), (14), (15), (21), and (22) and requiring continuity of E_z, E_y, H_z, and H_y at $x = b$ leads to the eigenvalue equations

$$\tan k_x b = -\frac{k_x}{i\sigma_x} \quad (25)$$

or

$$\tan k_x b = n^2 \frac{i\sigma_x}{k_x}. \quad (26)$$

For guided modes we have

$$i\sigma_x = \eta, \quad (27)$$

with real positive η.

Equation (25) is the eigenvalue equation for odd TE modes of a slab waveguide, while (26) is the eigenvalue equation for even TM modes of the slab.[4] When the amplitude coefficients of the superpositions of the TE and TM modes (3), (4), (7), and (8) (that are determined with the help of the boundary conditions) are substituted into the field expressions, we obtain for the field in the fiber core belonging to (25)

$$E_z = -\frac{k_y}{\beta k_x} F \sin(k_x x) \cos(k_y y) e^{-i\beta z} \qquad |x| \leqq b \tag{28}$$

and

$$H_z = \frac{F}{\omega \mu_0} \cos(k_x x) \sin(k_y y) e^{-i\beta z} \qquad |x| \leqq b. \tag{29}$$

For this mode we have $E_x = 0$. Viewing this field from the boundary of the slab, $x = b$, we see that the normal electric field component vanishes. This is typical for TE modes of the slah waveguide so that it is not surprising that the propagation constant of this mode is determined by an eigenvalue equation of the TE type.

The mode belonging to (26) has the following z components:

$$E_z = \frac{k_x \beta}{n^2 k_y k^2} G \sin(k_x x) \cos(k_y y) e^{-i\beta z} \qquad |x| \leqq b \tag{30}$$

and

$$H_z = \frac{G}{\omega \mu_0} \cos(k_x x) \sin(k_y y) e^{-i\beta z} \qquad |x| \leqq b. \tag{31}$$

This mode has $H_x = 0$. With respect to the surface $x = b$, it is indeed a TM mode.

For simplicity, the fields outside the core are not stated. However, a good approximation to these field expressions is obtained by using (21) and (22) to extend the field (28) and (29) outside the core and similarly hy using (14) and (15) with the core fields (30) and (31).

For $t \neq 0$, the mode field of the single-material fiber can only be described by an infinite series of modes. However, we find a crude approximation by using only the first two terms in this series expansion and obtain an eigenvalue equation hy requiring that a certain wave impedance be matched at the interface $x = b$. We stated earlier that only those modes of our structure with vanishing normal field components at the metallic planes resemhle modes of the true single-material fiher. The mode field (28) and (29) with $E_z = 0$ has a strong normal component of the electric field. We thus limit ourselves to the horizontally polarized field and use (30) and (31) as a crude approxima-

tion. Note that the field (30) and (31) consists of a superposition of one TE mode [eqs. (3) and (4)] and one TM mode [eqs. (7) and (8)].

The wave impedance,

$$\frac{E_z}{H_y} = \frac{i\omega\mu_0 k_x}{n^2k^2} \tan k_x b, \tag{32}$$

ohtained from (30) and (31) does not depend on the y coordinate. Similarly, we use (14) and (15) to form

$$\frac{E_z}{H_y} = -\frac{\omega\mu_0\sigma_x}{n^2k^2 - \sigma_y^2}, \tag{33}$$

which is also independent of y. Since the tangential field components must he continuous at the houndary $x = b$ hetween the two regions, we require that (32) he equal to (33), ohtaining the following approximate eigenvalue equation for the horizontally polarized modes (of only a certain special symmetry) of the single-material fiher:

$$\tan k_x b = \frac{i\sigma_x}{k_x} \frac{n^2k^2}{n^2k^2 - \sigma_y^2}. \tag{34}$$

The parameter σ_y must be obtained as the solution of the eigenvalue equation (18). In the limit $t = 0$, (34) should reduce to (26). To see that the correct limit is ohtained, we use (19) to write

$$n^2k^2 - \sigma_y^2 = k^2 - \rho^2. \tag{35}$$

For $t = 0$, we ohtain from (18)

$$\rho = (2\mu - 1)\frac{\pi}{2d}. \tag{36}$$

For small values of the integer μ and $kd \gg 1$, we have $\rho \ll k$ so that (26) and (34) become indeed approximately the same. We do not get exact agreement, since we approximated the field outside the core hy (14) and (15) instead of using the exact field expressions. We see that our eigenvalue equation (34) is a good approximation in the two limiting cases, $t \to 0$ and $t \to d$. Once σ_y has heen determined from (18) we find $\eta = i\sigma_x$ from

$$\eta = \sqrt{\sigma_y^2 - k_x^2 - k_y^2}, \tag{37}$$

and (34) with the help of (9). The propagation constant β can then be ohtained from (5) or (16).

IV. DISCUSSION AND NUMERICAL EXAMPLES

Marcatili has shown by an approximate analysis[1] that the single-material fiber can be made to support only a single guided mode, even if its dimensions are large compared to the wavelength, if the ratio $(\pi/4)(bd/t^2)$ approaches unity. However, for large values of kd and large values of bd/t^2, the single-material fiber supports a large number of guided modes.

We are limiting our discussion to the lowest-order guided mode. Since the properties of the single-material fiber can be obtained adequately from the approximate solutions, it is our principal purpose to show how well the approximate solution (34) and Marcatili's approximate theory work, and to study the field distributions of the exact solution that cannot be obtained from the approximate analysis. As indicated earlier, we limit the discussion to the modes with horizontal polarizations ($E_y = 0$), since the vertically polarized modes ($E_x = 0$) are very strongly influenced by the presence of the perfectly conducting planes that were used only to simplify the analysis.* The analysis is further restricted to modes whose E_x component is a symmetric function in both x and y. The modes with other symmetries can be obtained similarly by using slab waveguide modes of the appropriate symmetries.

All the numerical examples shown here were computed for the following choice of parameters:

$$\begin{aligned} d/\lambda &= b/\lambda = 5 \\ n &= 1.5. \end{aligned} \tag{38}$$

The boundary conditions at the plane $x = b$ were satisfied by matching the fields at 10 points evenly distributed between $y/d = 0.05$ and $y/d = 0.95$. As a consequence, the field expansion uses 20 modes in each region, 10 TE modes and 10 TM modes. Adequate accuracy was obtained this way. However, an expansion using only 6 points to match the fields did not appear sufficiently accurate.

The computer program was written to solve, first, the eigenvalue equations (18) and (23) by an iterative search procedure. Next, the computer was instructed to use a large trial value for β and compute the normalized field amplitudes (12), (13), (20), and (24) as well as the matrix elements of the equations system resulting from the boundary conditions at the N matching points. Next, the system determinant was examined and β was decreased until the determinant changed its

* The case of vertically polarized modes can be treated by replacing the electrical short-circuit planes with magnetic short circuits.

sign. By narrowing the increments for β successively and oscillating around the point where the sign change of the determinant occurred, an approximate solution for β was determined. Since the order of magnitude of the determinant was not known *a priori*, no attempt was made to reduce the value of the determinant below a certain limit. Once an approximate eigenvalue had been found, the coefficient $c_1^{(1)}$ was set equal to unity, and the first equation of the system was omitted. The remaining equation system was solved by inverting the reduced coefficient matrix. The values of the expansion coefficients were finally used to calculate the magnitude and direction of the electric field in a grid of preselected points in the x–y plane.

Figures 3 to 6 compare the magnitude of the electric field vector of the lowest-order mode of the single-material fiber with the magnitude of the field of the rectangular waveguide if $t/d = 0$. Figure 3 applies to a single-material fiber with the dimensions given by (38) and with $t/d = 0.32$. The magnitude of the field intensity is plotted as a function of x/b for different values of y/d. It is apparent that the field intensity decreases with increasing values of y. The field is strongest on axis and vanishes at $y = d$. In the absence of metallic planes, the field would not be zero at $y = d$, hut would decrease to a very small value. The solid curves indicate the field of the single-material fiber, while the hroken curves apply to the rectangular waveguide ($t = 0$). In the region of the guide where the support slab is present, $y/d < 0.32$, the field of the single-material fiber reaches out much further than the field of the corresponding rectangular waveguide, since it penetrates into the slah. For $y/d > 0.32$, the field shape of the single-material fiber has become identical with the field distribution of the rectangular waveguide.

Figure 4 shows the field distribution as a function of y/d for four different values of x/d. The solid curves describe again the field of the single-material fiber, while the broken curves belong to the rectangular waveguide. In the y direction, both fields vanish at $y = d$ but, near the edge of the single-material fiber, its field intensity is quite different from the rectangular waveguide field. We have plotted the ratio of the field intensity to the maximum value (the value that the field assumes for each value of x/d) at $y/d = 0$. Far from the edge of the core, the single-material fiber field is identical to the field of the rectangular waveguide. However, near the edge, at $x/b = 1$, the field is strong in the region $0 < y/d < 0.32$, since it is allowed to penetrate into the support slab. But in the range $0.32 < y/d < 1$, where it encounters the dielectric interface, it is relatively much weaker. The field of the rectangular waveguide is likewise weak near the dielectric

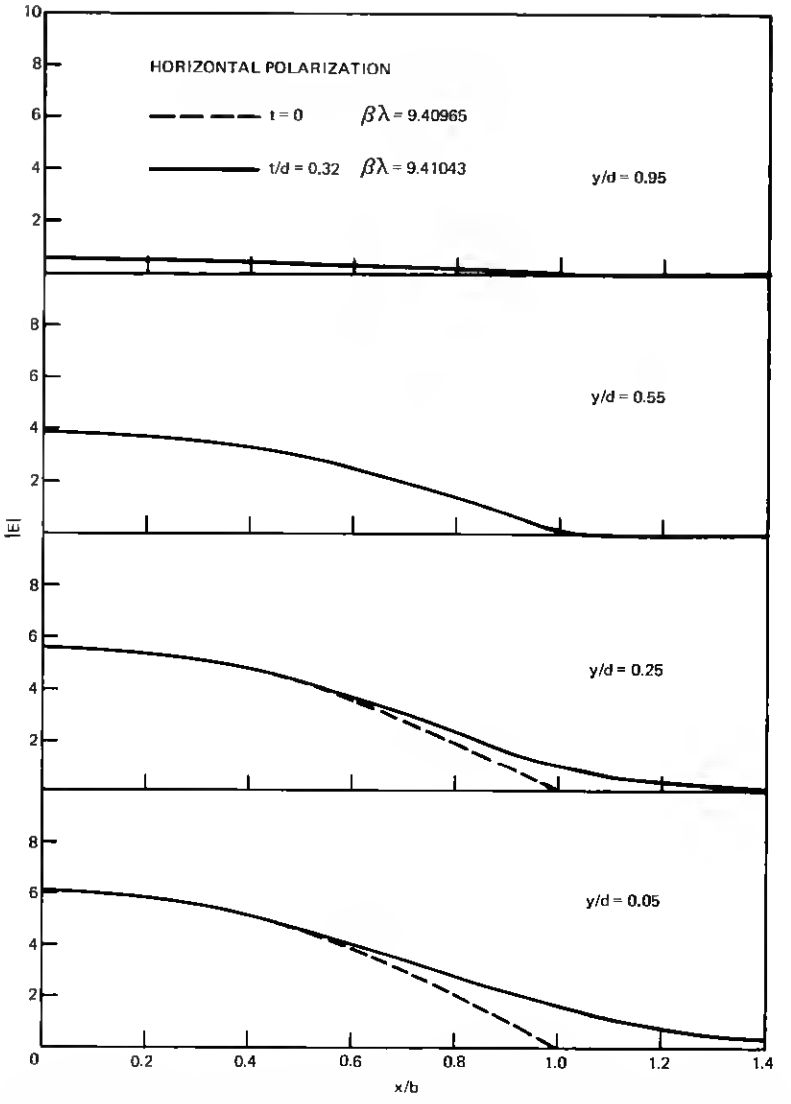

Fig. 3—Magnitude of the electric field vector shown as a function of the normalized horizontal dimension x/b. Solid curves describe the single-material fiber with $t/d = 0.32$, and broken curves apply to the fiber with $t/d = 0$.

interface; it appears strong only because of our normalization with respect to the maximum field intensity at $y/d = 0$. For $x/b > 1$, the rectangular waveguide field is no longer plotted since it decays rapidly to insignificant values outside the waveguide core. The single-material

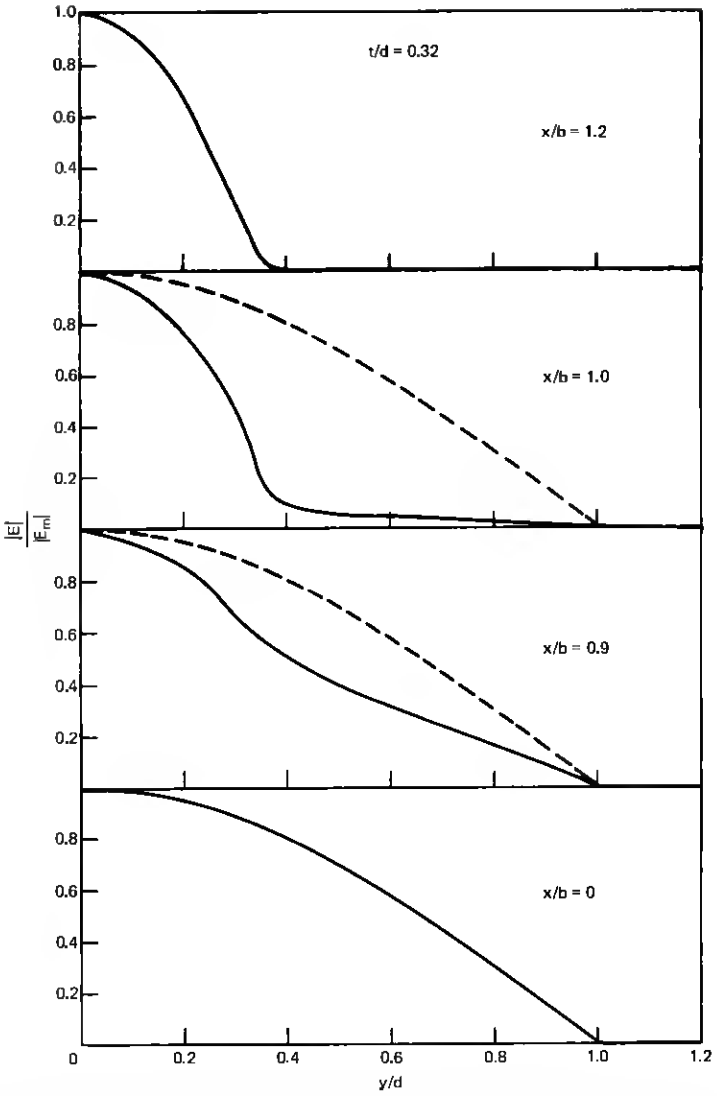

Fig. 4—Magnitude of the electric field vector relative to its maximum value at $y = 0$ as a function of the normalized vertical dimension y/d. Solid and broken curves describe the single-material fiber with $t/d = 0.32$ and $t/d = 0$.

fiber field shows the distribution typical of the lowest-order mode in the support slah.

Figures 5 and 6 show the same behavior for a single-material fiher with a much wider slah, $t/d = 0.8$. The field penetrates even further into the support slah, as can he seen from Fig. 5. However, the field

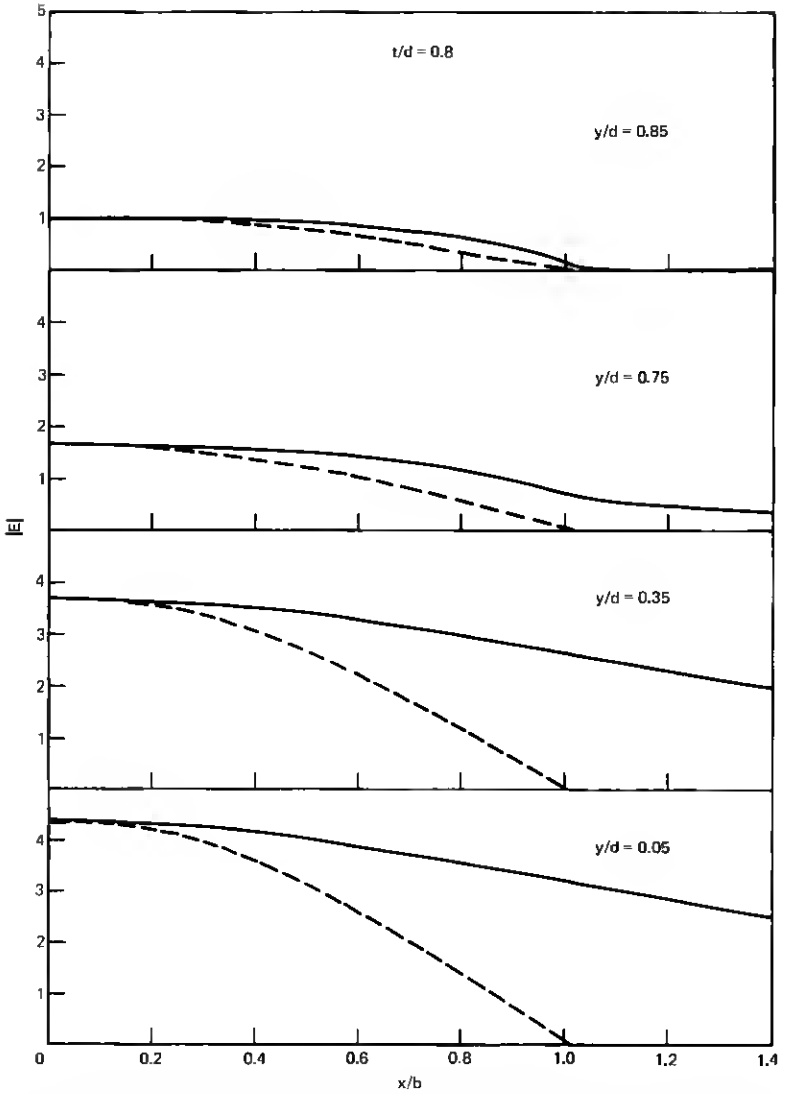

Fig. 5—Magnitude of the electric field vector shown as a function of the normalized horizontal dimension x/b. Solid curves describe the single-material fiber with $t/d = 0.8$, and the broken curves apply to the fiber with $t/d = 0$.

distribution in the vertical plane, shown in Fig. 6, is now much closer to the field distribution in the core of the rectangular fiber.

Figures 7 and 8 show the mode spectra for the single-material fiber with $t/d = 0.32$. Figure 7 presents the mode content of the field in the core. Because of our normalization, the square of the mode amplitudes

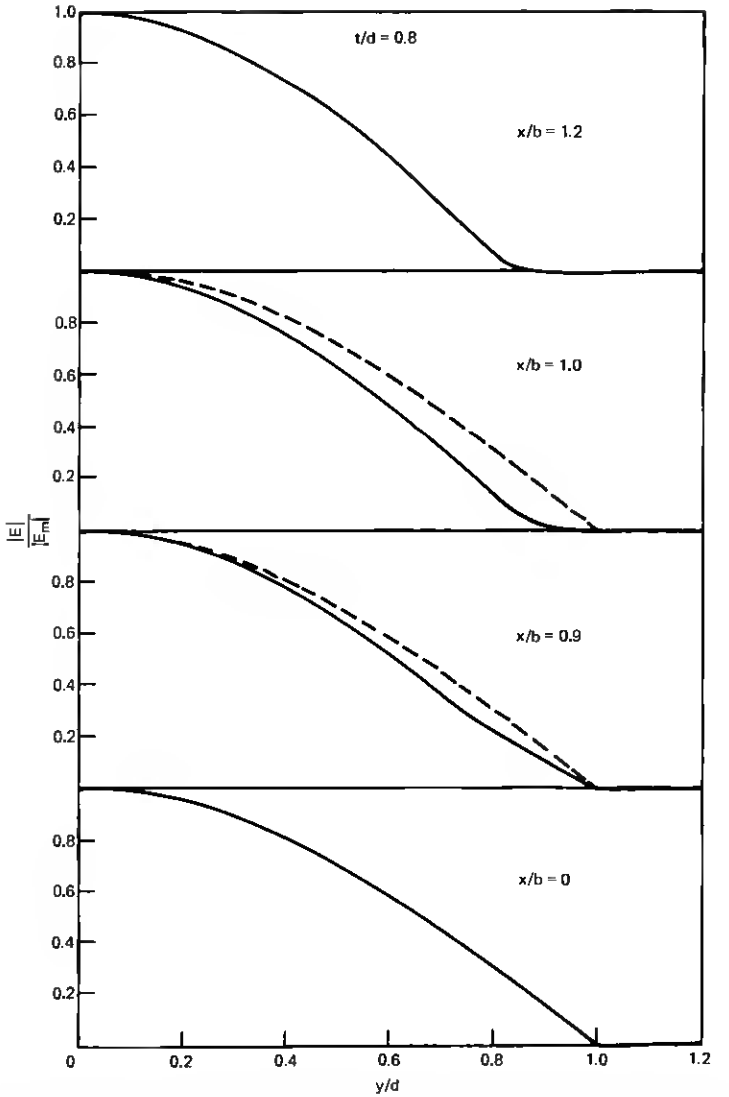

Fig. 6—Magnitude of the electric field vector relative to its maximum value at $y = 0$ as a function of the normalized vertical dimension y/d. Solid and broken curves describe the single-material fiber with $t/d = 0.8$ and $t/d = 0$.

$c_\nu^{(1)}$ represents the relative power carried by each mode of the series expansion (1) and (2). The broken vertical lines give the mode content of the corresponding mode of the rectangular waveguide. It is remarkable how nearly identical the mode amplitudes of the lowest-order TE and TM modes are in either case. Note that the mode amplitudes of

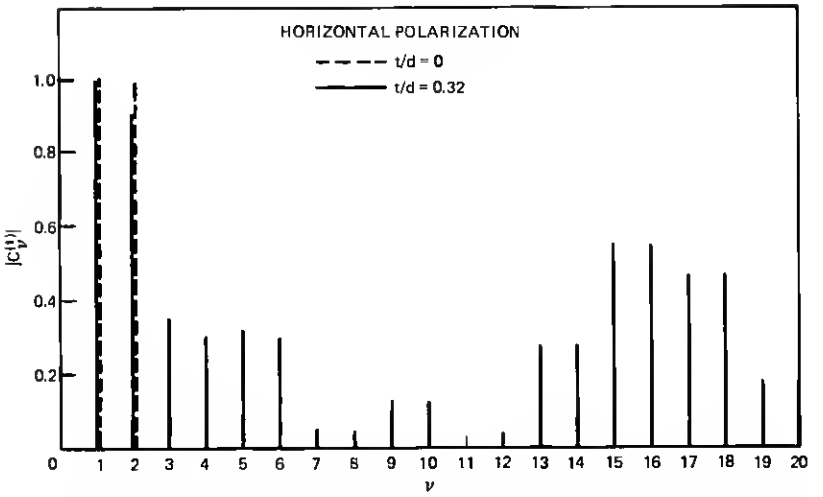

Fig. 7—Mode spectrum of the lowest-order single-material fiber mode inside its core. The solid vertical lines describe a fiber with $t/d = 0.32$, the broken vertical lines belong to the case $t/d = 0$.

the higher-order modes vanish because of the presence of the perfectly conducting planes; without them, the rectangular waveguide modes would also have to be represented by infinite-series expansions with a very slight mixture of higher-order modes. The mode of the single-material fiber consists of a mixture of the higher-order modes required

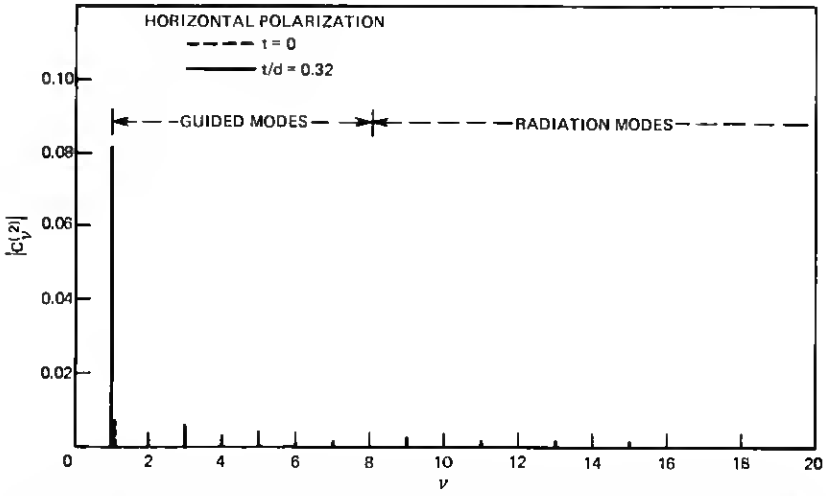

Fig. 8—Mode spectrum of the lowest-order single-material fiber mode in the region of its support slab with $t/d = 0.32$. The short vertical broken line represents the mode content of the fiber with $t = 0$.

to produce the field distortions in Figs. 4 and 6. The rise of the mode amplitudes for modes with $\nu > 12$ is not truly representative of the actual mode content. If the mode number is varied in the numerical approximation, it is found that, near the last mode, $\nu = N$, the mode amplitudes always tend to assume increased values. The appearance of the mode spectrum is thus somewhat dependent on the total number N of modes used in the series expansion. However, the distribution of lower-order modes was found to be very similar for $N = 16$ compared to the spectrum shown in Fig. 7 for $N = 20$. Only the highest-order modes appear with different amplitudes. When $N = 12$ was used, a different mode spectrum and an implausible field distribution was obtained, indicating insufficient accuracy.

Figure 8 shows the mode content of the field in the support slab. The mode amplitudes are much smaller, since much less power is carried outside the fiber core. The lowest-order TE mode is most prominent. The short broken line at $\nu = 1$ represents the much weaker contribution of the rectangular waveguide ($t = 0$). For our model, the lowest-order TM mode outside the core, $\nu = 2$, contributes slightly to the mode field of the rectangular dielectric waveguide, but its amplitude is too small to be visible on the scale of this figure. It is interesting that the field of the single-material fiber in the region of the support slab is represented to a very good approximation by the lowest-order TE mode of the support slab. The modes $\nu \leqq 8$ are guided slab modes with imaginary values of ρ_ν; modes with $\nu > 8$ have real valued parameters ρ_ν corresponding to the radiation modes of open slabs.

Figure 9 is a plot of the direction of the electric field vector in the vicinity of the corner of the dielectric material at $x/b = 1$, $y/d = 0.32$. Far from this corner, the field is horizontally polarized. It is remarkable how little distortion is evident near the dielectric discontinuity. There is no peak in the field intensity at the sharp dielectric corner, and the field direction is likewise almost unperturbed.

Finally, we present solutions of the eigenvalue equation (system determinant = 0). Instead of plotting values for the propagation constant β, we present values for the relative effective width of the fiber core. If the core boundary at $x = b$ were a metal wall we would have

$$k_x = \frac{\pi}{2b} \tag{39}$$

for the lowest-order mode. The actual values of k_x deviate from the value (39) partly because the dielectric discontinuity at $x = b$ is not an electrical short circuit, and also because the field penetrates some

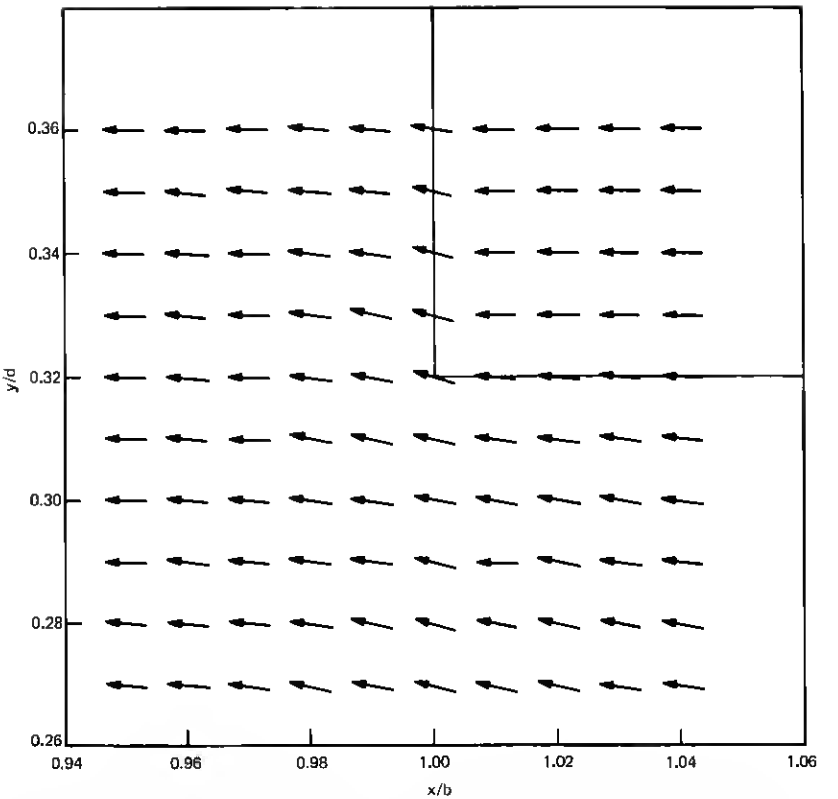

Fig. 9—Short arrows indicate the direction of the electric field vector of the lowest-order mode of the single-material fiber, with $t/d = 0.32$ near the corner of the dielectric material where the support slab is attached to the core.

distance into the support slab. We use the actual valuc of k_x to define an effective core width

$$b' = \frac{\pi}{2k_x}. \tag{40}$$

The value of k_x is obtained from the solution β of the eigenvalue equation with the help of (5) and (9)

$$k_x = \left[n^2k^2 - \beta^2 - \left(\frac{\pi}{2d} \right)^2 \right]^{\frac{1}{2}}. \tag{41}$$

The solid line in Fig. 10 represents the relative effective width of the core for the lowest-order mode of the single-material fiber with the

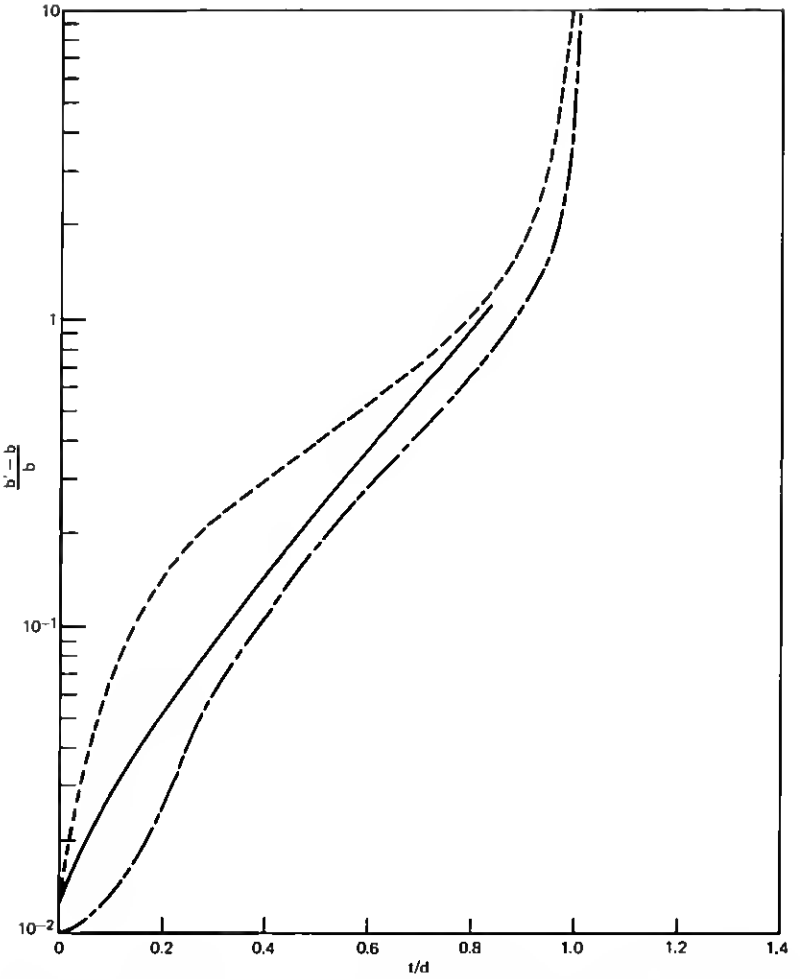

Fig. 10—Relative effective width of the core of the single-material fiber as a function of the relative thickness of its support slab t/d for the lowest-order mode. The solid line is the result of the numerical solution of the complete theory; the broken line was calculated from the solution of the approximate eigenvalue equation (34); and the dash-dot line is the result of Marcatili's theory.

dimensions stated in (38). This mode does not suffer a cutoff. It can propagate without power outflow into the support slab for arbitrarily small values of $1 - (t/d)$. The computer program had difficulties solving the eigenvalue problem for $t/d > 0.8$; thus, the solid curve is not continued beyond this point. The nonzero value of $(b' - b)/b$ at

$t/d = 0$ represents the field penetration of the rectangular waveguide mode outside the dielectric core.

The upper dotted line of Fig. 10 is the result of solving the approximate eigenvalue equation (34). For t/d near zero and near unity, the approximation is excellent. The departure of the approximation in the middle of the range is not surprising when we look at Fig. 4. The approximate solution uses the field distribution represented by the dotted line of Fig. 4, which is clearly a poor approximation of the actual field distribution. In fact, it is surprising how good the approximate solution for $(b' - b)/b$ is, even in this case. Even though the solid curve does not extend past $t/d = 0.8$, we can trust the dotted curve in this region, since the actual field distribution becomes very close to the approximate distribution. This is evident from a comparison of the solid and broken curves of Fig. 6.

The large error in the approximation in Fig. 10 causes only a very slight error for β. For $t/d = 0.32$, we obtain from the solid curve of Fig. 10 $(b' - b)/b = 0.1$ corresponding to $k_x\lambda = 0.2856$ or $\beta\lambda = 9.41043$. From the broken curve we obtain $(b' - b)/b = 0.24$, $k_x\lambda = 0.2534$ or $\beta\lambda = 9.41135$. The relative error in the β value is thus only $\Delta\beta/\beta = 0.01$ percent.

The dash-dot curve shown in Fig. 10 is a plot of eq. (15) of Ref. 1. This curve was plotted by using the following identification of the symbols in Ref. 1 with our symbols: $T = 2t$, $W = 2b$, and $H = 2d$. The dash-dot curve of Fig. 10 shows clearly how remarkably accurate Marcatili's approximate theory describes the effective width and hence the propagation constant of the single-material fiber mode. His approximation deviates more from the "exact" solution (given by the solid curve) near $t/d = 0$ and $t/d = 1$ than does the dotted curve. The disagreement near $t/d = 0$ is caused by assuming that the field must vanish at the boundary $x = b$ of the rectangular waveguide.

V. CONCLUSIONS

We have studied the properties of the lowest-order mode of the single-material fiber using a model that departs from the actual fiber by the presence of two perfectly conducting planes shown in Fig. 2. Horizontally polarized modes are not appreciably distorted by the presence of these planes. In particular, we are confident that the influence of the support slab on the field distribution and propagation constant of the single-material fiber mode is represented very accurately by this model. The agreement of the model with metallic planes and

tbe free single-material fiber becomes better for fibers witb large values of d/λ.

By representing the field of tbe single-material fiber as a superposition of tbe modes of the dielectric slabs in the core region and in the region of the supports, we find solutions by matching the boundary conditions in the plane $x = b$ at a finite number of points. We find tbat matcbing along 10 points in the range $0 < y/d < 1$ (requiring 20 modes in eacb region of the guide) provides satisfactory accuracy.

Tbis study sbows tbat tbe field of the single-material fiber in tbe vicinity of tbe edge, at $x = b$, departs considerahly from tbe field distrihution tbat would result for $t = 0$. However, for very narrow as well as very wide support slabs, a simple approximation using only the two lowest-order modes of the series expansion yields satisfactory results. Our tbeory thus serves tbe purpose of clarifying the range of applicability of approximate descriptions[1,2] of tbe single-material fiber and of inspiring confidence in tbe validity of such approximations.

In particular, it is our aim to sbow tbat Marcatili's approximate theory of the single-material fiber is indeed justified and yields very good results compared to our more precise treatment.

VI. ACKNOWLEDGMENT

The progress of tbis work was stimulated and influenced by a number of illuminating discussions with E. A. J. Marcatili.

APPENDIX

It is claimed that tbe analysis presented in this paper is an almost exact description of the single-material fiber, and yet the structure that is analyzed differs from tbe actual single-material fiber by tbe presence of tbe perfect metallic conductors attacbed to the fiber core, as shown in Fig. 2. In defense of this procedure, two remarks may be made bere.

The performance of the single-material fiber is dominated not by the dielectric-air interface on the two sides at $y = \pm d$ of the fiber core but by the presence of tbe attacbed support slabs. The electromagnetic fields of tbe single-material fiber modes extend much furtber into tbe support slabs tban tbey do into the air space outside tbe core, as sbown in Figs. 3 through 6. Tbe dielectric-air boundary acts almost like an electrical short circuit, so that the presence of actual short circuits at the dielectric-air interface at $y = \pm d$ has a very slight effect. In particular, it is tbe radiation of power into the support slabs rather than into the air space outside the core that signals the cutoff of tbe guided modes. Tbis behavior is described correctly by our analysis.

It is easy to estimate the field penetration into the air space above and below the core in the absence of the perfect conductors. The field outside the fiber is described by the functional dependence $\exp(-\gamma y)$. The decay parameter γ is defined as [see eqs. (1.2–14) and (1.3–44), Ref. 5]:

$$\gamma = \left[(n^2 - 1)k^2 - \left(\frac{\pi}{d}\right)^2 \right]^{\frac{1}{2}}. \tag{42}$$

With the numbers used in the numerical example, we obtain $\gamma\lambda = 7$. This means that, at a distance of $\lambda/7$ from the air-dielectric interface, the field has decayed to $1/e^2$ (or 14 percent) of its power density at the interface. Instead of having an effective electric short circuit at this distance, the presence of the metallic planes moves the short circuit a relative distance of 1.4 percent (in terms of the fiber diameter) nearer to the fiber core. This small change of the electrical width of the core has only a very slight effect on the field penetration into the slabs, which is the most interesting feature of the single-material fiber. Furthermore, this change can be taken into account by allowing the value $2d$ of the modified fiber to be 3 percent larger than that of the actual fiber.

The cutoff condition of the modes follows from the eigenvalue equation, which is the condition for the vanishing determinant of the equation system resulting from the continuity requirements for the tangential field components. At cutoff, the propagation constant β ceases to have real solutions, but becomes complex. No analytical expression can be given for the cutoff point. Its determination from the numerical analysis is difficult. In this respect, the approximate theory proves to be more powerful, since it is able to estimate the cutoff point.

REFERENCES

1. E. A. J. Marcatili, "Slab-Coupled Waveguides," B.S.T.J., *53*, No. 4 (April 1974), pp. 645–674.
2. P. Kaiser, E. A. J. Marcatili, and S. E. Miller, "A New Optical Fiber," B.S.T.J., *52*, No. 2 (February 1973), pp. 265–269.
3. P. Kaiser and H. W. Astle, "Low-Loss Single Material Fibers Made from Pure Fused Silica," B.S.T.J., *53*, No. 6 (July-August 1974), pp. 1021–1039.
4. D. Marcuse, *Light Transmission Optics*, New York: Van Nostrand Reinhold Co., 1972.
5. D. Marcuse, *Theory of Dielectric Optical Waveguides*, New York: Academic Press, 1974.